
This is an electronic reprint of the original article.
This reprint may differ from the original in pagination and typographic detail.

Li, Yongming; Ma, Xikui; Wang, Xuchen; Tretyakov, Sergei
Going beyond perfect absorption: Superdirective absorbers

Published in:
Physical Review Applied

DOI:
[10.1103/PhysRevApplied.21.054060](https://doi.org/10.1103/PhysRevApplied.21.054060)

Published: 01/05/2024

Document Version
Publisher's PDF, also known as Version of record

Please cite the original version:
Li, Y., Ma, X., Wang, X., & Tretyakov, S. (2024). Going beyond perfect absorption: Superdirective absorbers. *Physical Review Applied*, 21(5), Article 054060. <https://doi.org/10.1103/PhysRevApplied.21.054060>

This material is protected by copyright and other intellectual property rights, and duplication or sale of all or part of any of the repository collections is not permitted, except that material may be duplicated by you for your research use or educational purposes in electronic or print form. You must obtain permission for any other use. Electronic or print copies may not be offered, whether for sale or otherwise to anyone who is not an authorised user.

Going beyond perfect absorption: Superdirective absorbers

Yongming Li^{1,2,*}, Xikui Ma,¹ Xuchen Wang³, and Sergei Tretyakov²

¹State Key Laboratory of Electrical Insulation and Power Equipment, School of Electrical Engineering, Xi'an Jiaotong University, Xi'an, 710049, China

²Department of Electronics and Nanoengineering, Aalto University, P.O. Box 15500, FI-00076 Espoo, Finland

³Institute of Nanotechnology, Karlsruhe Institute of Technology, P.O. Box 3640, 76021 Karlsruhe, Germany

 (Received 19 February 2024; revised 12 April 2024; accepted 7 May 2024; published 29 May 2024)

In the context of electromagnetic absorption, it is obvious that for an infinite planar periodic structure illuminated by a plane wave the maximum attainable absorptance, i.e., perfect absorption, is theoretically limited to 100% of the incident power. Here we show that an intriguing possibility of overcoming this limit arises in finite-sized resonant absorbing arrays. We present a comprehensive analysis of a simple two-dimensional strip array over an infinite perfectly conducting plane, where the strips are loaded with bulk-impedance loads. The absorptance is defined as the ratio of the dissipated power per unit length of the strips to the incident power on a unit length of the array width. The results show that even regular subwavelength arrays of impedance strips can slightly overcome the limit of 100% absorptance, while with use of aperiodic arrays with optimized loads, absorptance can be significantly increased as compared with the scenario where the strips are identical. In principle, by tuning of the bulk loads, high superunity absorptance can be realized for *all* angles of illumination.

DOI: [10.1103/PhysRevApplied.21.054060](https://doi.org/10.1103/PhysRevApplied.21.054060)

I. INTRODUCTION

Absorbers for electromagnetic waves have a pivotal role in various applications, such as energy harvesting [1], stealth technology [2,3], and sensors [4,5]. In the literature, absorbers are called “perfect” if they absorb all the power incident on their surface, at least at a specific frequency and angle of incidence. Motivated by the variety of applications, many studies have been conducted on perfect absorbers, in particular, exploiting metagratings, metasurfaces, or metamaterials [6–11]. Reference [10] provides a tutorial overview on the phenomenon of perfect absorption in infinite optically thin planar layers and classifies perfect absorbers according to their operational principles. For an infinite periodic structure illuminated by a propagating plane wave, the maximum absorptance is obviously 100%. However, the absorptance of finite-sized bodies can sometimes exceed 100%. This typically occurs when these absorbers work at the conjugate-impedance-matching condition to maximize the received power [12,13]. Higher than 100% absorptance means that the absorber can capture and absorb more power than is incident on its geometric cross section. This means that the ideal black body that was introduced in 1860 by Kirchhoff [14] is not the ultimate absorber, although it absorbs all the incident rays falling on its surface. In particular, small resonant particles,

for example, subwavelength-sized metallic particles, are able to absorb significantly more than a black body of the same size (see, e.g., Refs. [12,15–18]). Essentially, these resonant particles have the capability to gather the power of the incident wave from an area significantly exceeding the physical cross section of the particles. Similarly, in the antenna theory, the upper limit of the effective area of a resonant dipole is $(3/8\pi)\lambda^2$, where λ is the corresponding working wavelength [16]. This value is independent of the dipole size, which means that no upper limit of the absorption cross section exists if multipolar resonant modes of the object are permitted (see, e.g., Refs. [18–21]). Most superabsorption research focuses on small particles rather than on electrically large bodies. While theoretically there is no limit on how large the absorption cross section can be, and some approaches to physical realizations of large superabsorbing bodies have been proposed (see, e.g., Refs. [13,18]), these approaches would require the filling of bulk bodies by complex media with highly resonant and extremely-low-loss microstructures.

Conventional realizations of thin resonant absorbers are based on metasurfaces, most commonly in the form of multielement resonant arrays [10]. It is believed that such electrically large but finite-sized absorbing metasurfaces and multielement resonant arrays perform similarly to corresponding infinite-sized structures in terms of absorption efficiency, absorbing a maximum of 100% of the power incident on their surfaces. Truncated (finite-sized) periodic

*Corresponding author: yongmingli@stu.xjtu.edu.cn

structures, as a specific type of multielement resonant array, are often regarded as practically the simplest and most-effective realizations of thin resonant absorbers. Researchers have rarely explored the difference between infinite-sized periodic absorbers and finite-sized, truncated ones. Moreover, to the best of our knowledge, it is not known if it is possible to increase the effective area above 100% of the geometric size and what is required for the realization of such extreme properties of absorbing metasurfaces.

In the work reported in Ref. [22], we realized superdirective reflectors by locally optimizing the current distribution, as the densely arranged strip array supports surface modes. Consequently, this arrangement gives rise to an increased effective cross section relative to the physical size. Motivated by that work, here we examine a simple, analytically solvable example of a two-dimensional array of impedance strips and present two distinctive absorbers based on finite-length arrays. One scenario concerns the truncated periodic array where all the strips are loaded with identical impedance loads, while the other focuses on arrays with globally optimized load impedances. Both these absorbers exhibit absorptance that exceeds 100% for a certain angle of plane-wave incidence. Our results show that optimization of load impedances globally can enable absorption of more incident power as compared with the case for conventional finite-width regular arrays. This research reveals that it is possible for absorber designs to go beyond “perfect absorption” in electrically thin metasurfaces.

II. PRINCIPLE AND METHOD

We consider geometrically periodic strip arrays placed over a perfectly electrically conducting (PEC) ground plane at distance h . The strips are periodically loaded with impedance loads with the impedances per unit length equal to Z_L (Ω/m). The distance between the insertions l is electrically small, so the loaded strips can be considered as effectively uniform-impedance strips.

As the reference case and the initial design step, we first consider an infinite periodic array, where all the load impedances Z_L are identical. The array is illuminated by a TE-polarized plane wave $\mathbf{E}_{\text{inc}} = E_0 e^{-jk_0 \sin \theta_i y - jk_0 \cos \theta_i z} \hat{x}$, where $k_0 = \omega_0 \sqrt{\epsilon_0 \mu_0}$ is the wave number in free space; see the illustrations in Figs. 1(a) and 1(b). The reflected wave from the ground plane is given by $\mathbf{E}_{\text{ref}} = -E_0 e^{-jk_0 \sin \theta_i y + jk_0 \cos \theta_i z} \hat{x}$. This is one of the simplest examples of thin metasurface absorbers (see Ref. [10]). For such an infinite-sized periodic structure, transmission-line theory can be conveniently used [23], and the equivalent circuit is depicted in Fig. 1(c).

For simplicity of analysis, we assume that the array is in free space. According to Ref. [24], the input impedance of the grounded substrate is given by

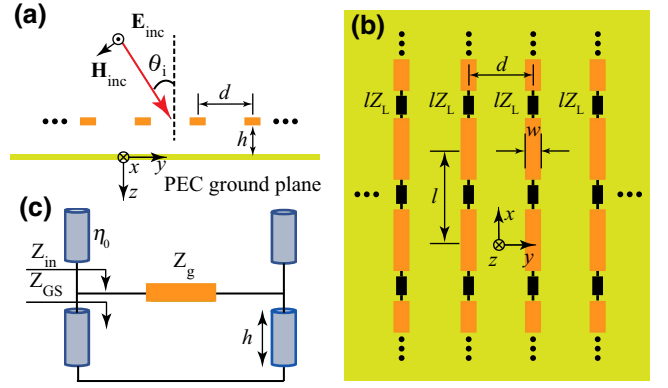


FIG. 1. (a) Front view of an infinite periodic strip array placed over an infinite ground plane and illuminated by a plane wave traveling in the direction of θ_i . The distance between the two adjacent strips is d . (b) Top view of the array. The strips are loaded with bulk impedances inserted periodically with period l . The width of the strips is w . Both l and w are much smaller than the wavelength in free space. The periodically loaded strips can be modeled as homogeneous-impedance strips with impedances per unit length Z_L . (c) Equivalent circuit of the system.

$Z_{\text{GS}} = j \tilde{Z}_0 \tan(k_0 h \cos \theta_i)$, where $\tilde{Z}_0 = \eta_0 / \cos \theta_i$ represents the characteristic impedance for TE-polarized plane waves for incident angle θ_i , where η_0 is the free-space impedance. The input impedance of the whole structure is the parallel connection of Z_{GS} and the grid impedance Z_g of the strip array; that is, $Z_{\text{in}} = Z_{\text{GS}} \parallel Z_g$. The equivalent grid impedance of a densely periodic strip array reads [23, Eq. 4.38]

$$Z_g = Z_L d + j \frac{\eta_0}{2} \alpha_{\text{ABC}}, \quad (1)$$

where the grid parameter $\alpha_{\text{ABC}} = k_0 d / \pi \log(d / (2\pi r_{\text{eff}}))$ (see Ref. [23, Eq. 4.32]), and the effective radius $r_{\text{eff}} = w/4$. To realize perfect absorption, the input impedance of the infinite structure should match the impedance of free space for the incident wave. The required load impedance for the designed incident angle θ_i is determined by

$$Z_L = \frac{1}{d} \left(\frac{Z_{\text{GS}} \tilde{Z}_0}{Z_{\text{GS}} - \tilde{Z}_0} - j \frac{\eta_0}{2} \alpha_{\text{ABC}} \right). \quad (2)$$

For an infinite strip array, the induced currents flowing on the strips are calculated by

$$I_{\text{inf}} = \frac{2(E_{\text{ref}} - RE_{\text{inc}})}{\tilde{Z}_0(1 - e^{-jk_0 2h \cos \theta_i})} d, \quad (3)$$

where the reflection coefficient R for a TE-polarized plane wave reads $R = (Z_{\text{in}} - \tilde{Z}_0) / (Z_{\text{in}} + \tilde{Z}_0)^{-1}$. The induced currents at infinite-strip-array absorbers, given by Eq. (3),

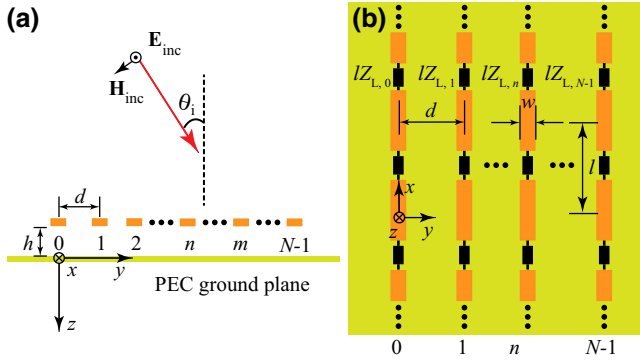


FIG. 2. (a) Finite-width strip array above an infinite PEC ground plane under illumination by a TE-polarized plane wave at θ_i . (b) Top view of the structure. The first strip is at the position $y = 0, z = -h$.

are used later for comparison with those of finite-sized absorbers.

In practice, designed periodic arrays need to be truncated to finite-sized structures. The corresponding finite-sized strip array is shown in Figs. 2(a) and 2(b). In finite arrays, it makes sense to use different load impedances for different strips as a means to optimize absorption. The truncated periodic array is a special case when all the loads are still the same, $Z_{L,n} = Z_L$ with $n = 0, 1, \dots, N-1$. When such a finite-sized structure is excited by a plane wave, the induced current I_m that flows on the surface of the m th strip dissipates Joule heat in lossy loads. We define the absorptance A of the finite-sized structure as

$$A = \frac{P_{\text{dis}}}{P_{\text{inc}}}, \quad (4)$$

where the dissipated power is given by

$$P_{\text{dis}} = \frac{1}{2} \sum_{m=0}^{N-1} |I_m|^2 \text{Re}\{Z_{L,m}\} \quad (5)$$

and the incident power on the array's geometric area (per unit length along the x axis) is given by $P_{\text{inc}} = E_0^2 N d / (2\tilde{Z}_0)$. This definition is used to evaluate whether the designed absorber has a superdirective property. If the absorptance is greater than 100%, this means that the designed absorber is a superdirective absorber, as it absorbs more power than is falling on its surface.

For finite-sized absorbing arrays, the total external electric field $E_x^{\text{ext}}(y, z) = -j2E_0 \sin(k_0 \cos \theta_i z) e^{-jk_0 \sin \theta_i y}$ at the coordinate (y, z) is the superposition of the incident wave and its reflection from the ground plane. For a given set of load impedances $\vec{Z}_L = (Z_{L,0}, Z_{L,1}, \dots, Z_{L,N-1})^T$, the induced current can be easily obtained by a simple matrix

operation according to [22, Eq. (5)]

$$\vec{I} = \vec{\bar{Z}}^{-1} \cdot \vec{U}, \quad (6)$$

where the column vector of the induced currents is represented by $\vec{I} = [I_0, I_1, \dots, I_{N-1}]^T$, while the total-external-voltage vector is represented by $\vec{U} = [E_x^{\text{ext}}(y_0, -h), E_x^{\text{ext}}(y_1, -h), \dots, E_x^{\text{ext}}(y_{N-1}, -h)]^T$. $\vec{\bar{Z}} = \vec{\bar{Z}}_s + \vec{\bar{Z}}_m + \vec{\bar{Z}}_L$ is the impedance matrix, which is composed of the self-impedance matrix (a diagonal matrix) $\vec{\bar{Z}}_s = \text{diag}(Z_0, Z_1, \dots, Z_n, \dots, Z_{N-1})$, the load-impedance matrix $\vec{\bar{Z}}_L = \text{diag}(\vec{Z}_L)$, and the mutual-impedance matrix $\vec{\bar{Z}}_m$. In the self-impedance matrix, $Z_n = k_0 \eta / 4 [H_0^{(2)}(k_0 r_{\text{eff}}) - H_0^{(2)}(2k_0 h)]$ is the self-impedance of strip n , and for the mutual-impedance matrix, $Z_{nm} = k_0 \eta / 4 [H_0^{(2)}(k_0 |y_m - y_n|) - H_0^{(2)}(k_0 \sqrt{(y_m - y_n)^2 + 4h^2})]$ is the mutual impedance between strips m and n . With knowledge of the induced currents, the absorptance and dissipated power can be found from Eqs. (4) and (5), respectively. In this work, the example operation frequency is chosen as $f_0 = 10$ GHz. The distance between the adjacent strips satisfies $d = \lambda_0 / 8$, where λ_0 is the wavelength in free space, and the distance h from the ground plane is set as $\lambda_0 / 6$. The effective radius r_{eff} is equal to $\lambda_0 / 100$. The time dependence is assumed to follow $e^{j\omega t}$. For the main example of finite-sized absorbers, the array size is set to $13.5\lambda_0$, which corresponds to $N = 108$.

III. NUMERICAL RESULTS

For an infinite array, the required load impedance for perfect absorption, corresponding to various designed incident angles, is calculated by Eq. (2). For two specific examples, one for normal incidence and the other for oblique incidence with $\theta_i = 80^\circ$, the required load impedances Z_L for perfect absorption in the designed direction are $(7.5347 \times 10^4 - j5.2139 \times 10^4) \Omega/\text{m}$ and $(1.8921 \times 10^4 - j1.1154 \times 10^5) \Omega/\text{m}$, respectively.

The absorptance for such an infinite-sized strip array can be calculated analytically as $1 - |R|^2$, since there is no transmission. Here, results are obtained with COMSOL MULTIPHYSICS. The absorptance as a function of the incident angle is depicted as a dashed black curve in Figs. 3(a) and 3(b) for the designed two specific examples. It can be observed that the maximum absorptance is 100%, which occurs in the designed directions of 0° and 80° , respectively. Obviously, the unity absorptance is the maximum attainable value for any infinite passive periodic structure illuminated by a plane wave.

The induced current flowing on the surface of the infinite-sized strip array is calculated by Eq. (3). For normal incidence, $I_{\text{inf}} = j1.1494 \times 10^{-5}$ A, both the

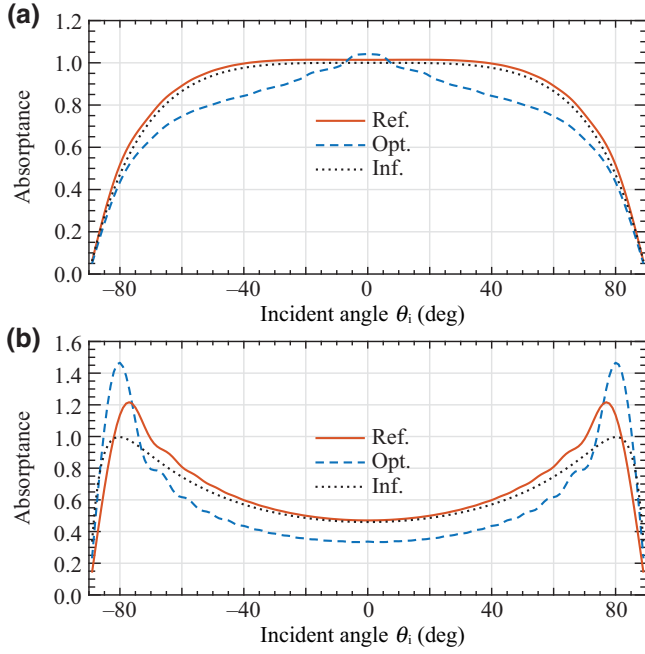


FIG. 3. Absorbance as a function of the incident angle θ_i for a designed incident angle of (a) 0° and (b) 80° . For finite-sized absorbers, the solid red curve indicates the reference case (Ref.; all the load impedances are the same as for the designed periodic infinite array), while the dashed blue curve shows the optimized case (Opt.; the optimized loads). The dotted black curve shows the absorbance of the designed infinite absorber (Inf.).

amplitude and the phase of the induced current are constant numbers. For oblique incidence at $\theta_i = 80^\circ$, $I_{\text{inf}} = j9.5579 \times 10^{-6}$ A, the amplitude is a constant number, while the phase varies linearly, as $e^{-jk_0 \sin \theta_i y}$. The induced-current distribution is depicted in Figs. 4(a) and 4(b) for $\theta_i = 0^\circ$ and $\theta_i = 80^\circ$, respectively. In the perfect-absorption regime, the specularly reflected wave from the PEC ground plane is eliminated by the field generated by the infinite array of induced currents [10], while the power carried by the incident wave is fully dissipated by the lossy-load impedances.

In practical designs, the infinite periodic array is truncated into a finite-sized strip array where all elements are loaded with identical impedance loads, calculated from the theory of infinite arrays. The corresponding load impedance is obtained from Eq. (2). For such a truncated finite-sized strip array, the absorbance defined in Eq. (4) as a function of the incident angle θ_i is depicted in Figs. 3(a) and 3(b) for the arrays designed to function as perfect absorbers for incident angles $\theta_i = 0^\circ$ and $\theta_i = 80^\circ$, respectively. We observe that for the designed incident angle, the absorbance does not have the value of unity. When the incident angle equals 0° and 80° , the absorbance calculated by Eq. (4) for the reference arrays is 101.4% and 113.6%, respectively. With the increase of the incident

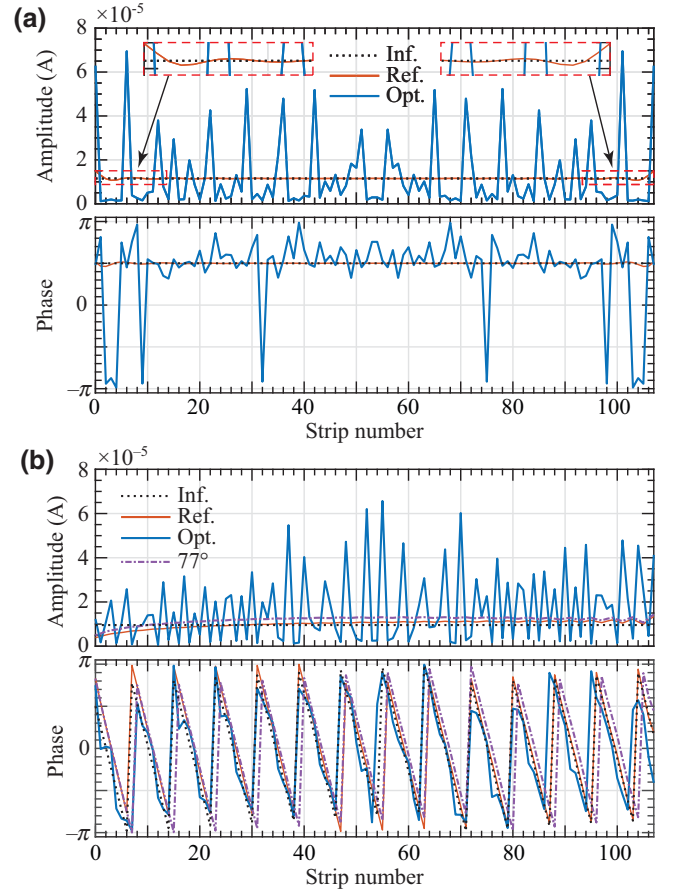


FIG. 4. Induced-current distribution for two designed incident angles θ_i of (a) 0° and (b) 80° . The dotted black curve corresponds to infinite absorbers (Inf.). For finite-sized absorbers, the solid red curve and the solid blue curve represent the reference case (Inf.; connected with identical loads) and the optimized case (Opt.; connected with optimized loads), respectively. The dot-dashed purple curve in (b) represents the induced-current distribution when the incident plane wave is traveling from 77° .

angle, the absorbance at the designed incident angle shows an increasing trend.

For a better understanding of the superabsorption mechanism, the induced-current distributions are depicted in Figs. 4(a) and 4(b) for $\theta_i = 0^\circ$ and $\theta_i = 80^\circ$, respectively. Compared with the infinite array, in the finite-sized array the induced currents are different, especially at the edges of the strip array. We first compare the performance of infinite and truncated periodic arrays. For the normal-incidence case, the results in Fig. 3 show that even the reference finite-sized absorber exhibits a slightly superdirective (above-100%) absorbance. This is a counterintuitive result because in this case all the array elements are the same as in the corresponding infinite array. This result can be explained by the particularities of the current distribution over the absorber area. Over the central area of the array, the amplitude and phase vary slowly and have

nearly the same values as in the case of the corresponding infinite periodic array. However, close to the array edges, the induced-current amplitude is higher; see the insets in Fig. 4(a). Higher current amplitude corresponds to higher absorption in the elements that are close to the edges, resulting in a slight increase of the total absorbed power. Distribution of induced currents in dense wire arrays was studied earlier for semi-infinite arrays of ideally conducting wires in free space [25], where a similar increase of the current amplitude at the edge was also noticed. However, for normal incidence, this effect of increased absorption in regular arrays is rather small and in practice can possibly be ignored.

As is seen from Fig. 4(b), absorbing arrays designed for oblique angles show much more-pronounced superdirective absorption. For nearly grazing incidence at $\theta_i = 80^\circ$, the amplitude of the induced currents at a finite-sized array shows an increasing trend along the $+y$ direction. The induced currents on most of the strips are greater than induced currents observed for the infinite array, particularly toward the ends of the array. The maximum absorptance is 121.6%, which occurs in the direction corresponding to $\theta_i = 77^\circ$. Note that the load impedance at the corresponding infinite array was found for $\theta_i = 80^\circ$. The induced currents in this case, shown by the dot-dashed purple curve in Fig. 4(b), are larger than the currents induced by the wave incident at $\theta_i = 80^\circ$, which means more dissipated power. The maximum-absorptance direction deviation from the designed direction is caused by the influence of the element pattern. Although the array factor always aligns accurately with the desired direction, there is a slight shift in the product of the array factor and the element pattern. This shift is toward smaller angles, due to the increased effective cross section ($\cos \theta$ is larger). As the size of the array increases, the array factor becomes more directive [22]. This can also be observed and validated in Fig. 5, which shows the absorptance as a function of incident angle for absorbers of different sizes. With the increasing length of the strip array, the absorptance of regular arrays decreases. The absorptance will ultimately tend to unity, which is the case of conventional perfect absorption for the infinite structures. This result confirms that the main mechanism of superabsorption in finite-sized regular arrays is due to edge effects.

Motivated by the results in Ref. [22] that showed a possibility to realize superdirective anomalous reflectors with use of subwavelength arrays with optimized loads, we next use optimization techniques to design absorbing arrays. As a reference for comparison, we use the results discussed above for finite-sized absorbers formed by truncation of conventional uniform perfect absorbers.

Here, a genetic algorithm, a global optimization method, is used to find the optimal load impedances. The objective function is defined as $\mathcal{O} = \min\{-P_{\text{dis}}\}$; that is, the goal is to dissipate as much incident power as possible.

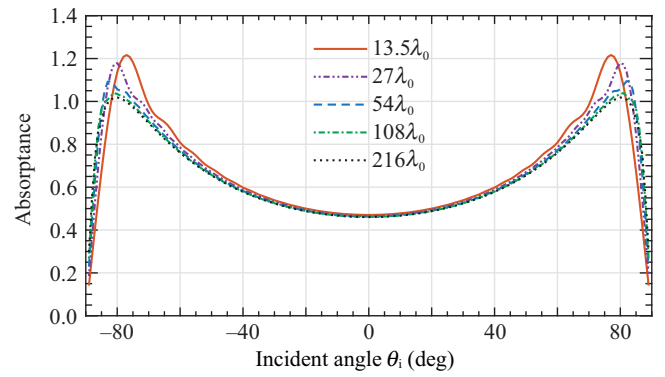


FIG. 5. Absorptance as a function of incident angle θ_i for different-sized strip arrays, where the designed angle of incidence is 80° .

The absorptance of the optimized arrays as a function of the incident angle is shown by dashed blue curves in Figs. 3(a) and 3(b) for $\theta_i = 0^\circ$ and $\theta_i = 80^\circ$, respectively. The absorptance for normal incidence is 104.2%, while it reaches a value as high as 146.6% for the large-incident-angle example. Comparison with the reference case of truncated regular arrays and the optimized array shows that after optimization the absorptance can be significantly increased, especially when the incident wave has an extreme incident angle. The current distribution in the optimized case becomes highly irregular (see the solid blue curves and dotted black curves in Fig. 4), corresponding to a high level of excited evanescent fields in the array vicinity. Also in this case we observe a tendency of higher induced currents close to the array edges. However, increased absorption at normal incidence leads to weaker absorption at other angles. The load impedances required to realize the required induced currents of the reference case and the optimized case are presented in Figs. 6(a) and 6(b) for incident angles of 0° and 80° , respectively.

COMSOL MULTIPHYSICS is used to calculate the scattered electric field and illustrate the superabsorption effect when the incident angle is 80° . The configuration for COMSOL MULTIPHYSICS is depicted in Fig. 7(a). The real part of the scattered electric field is depicted in Figs. 7(b) and 7(c). Figure 7(b) corresponds to the reference case of a truncated uniform strip array [see the blue lines in Fig. 6(b)]. Compared with Fig. 7(b), a wider shadow region can be observed in Fig. 7(c), where the strips are loaded with the optimized loads [see the red curves in Fig. 6(b)]. A wider shadow means that more power has been dissipated in the lossy loads; that is, the absorptance and the effective absorption width are greater. On the surface of the optimized superdirective absorber we see strong surface-wave fields, which confirms that the main mechanism of such superabsorption is the optimized excitation of evanescent waves in the vicinity of the array. Although the geometric-cross-section area is small at oblique angles,

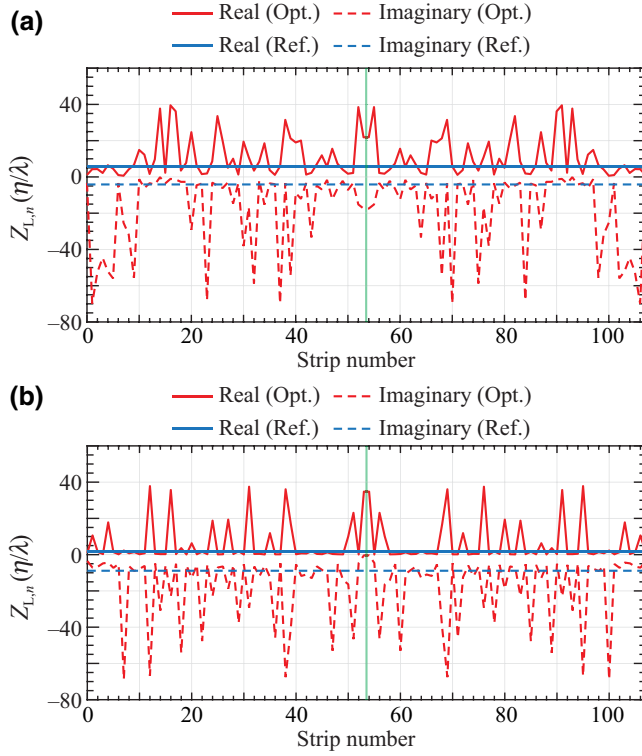


FIG. 6. Load-impedance distributions for two designed incident angles: (a) $\theta_i = 0^\circ$ and (b) $\theta_i = 80^\circ$. The red curves show the load impedances of the optimized loads (Opt.), while the blue curves represent the values of the reference (Ref.) load impedance. The solid and dashed curves represent the real and imaginary parts of the load impedance, respectively. The solid green line shows the symmetry axis of the strip array.

the excited surface waves carry power over the whole area of the array, where it is dissipated in the optimized resistive loads of the array elements.

Superdirective arrays usually have a narrow frequency bandwidth due to fast variations of the currents and associated high-amplitude reactive fields. Because also in the optimized absorbers we observe fast variations of the induced currents, we next investigate the frequency bandwidth of absorption, comparing the frequency response of the optimized and reference absorbers of different sizes. To find the frequency response of the designed structures, one needs to define the frequency dependence of the load impedances as passive bulk loads. We assume that the load resistances do not depend on the operation frequency, $\text{Re}\{Z_{L,n}\} = R_n$, while the reactive (capacitive) parts of the load impedances $\text{Im}\{Z_{L,n}\}$ depend on the operation frequency as that of capacitors: $\text{Im}\{Z_{L,n}\} = (-2\pi f C_n)^{-1}$. The load capacitances C_n are found by our setting them to the values that correspond to the required reactances $\text{Im}\{Z_{L,n}\}$ at the design frequency f_0 . Then we model the loads in COMSOL MULTIPHYSICS as capacitors and resistors, so that the frequency response of the structure can be calculated.

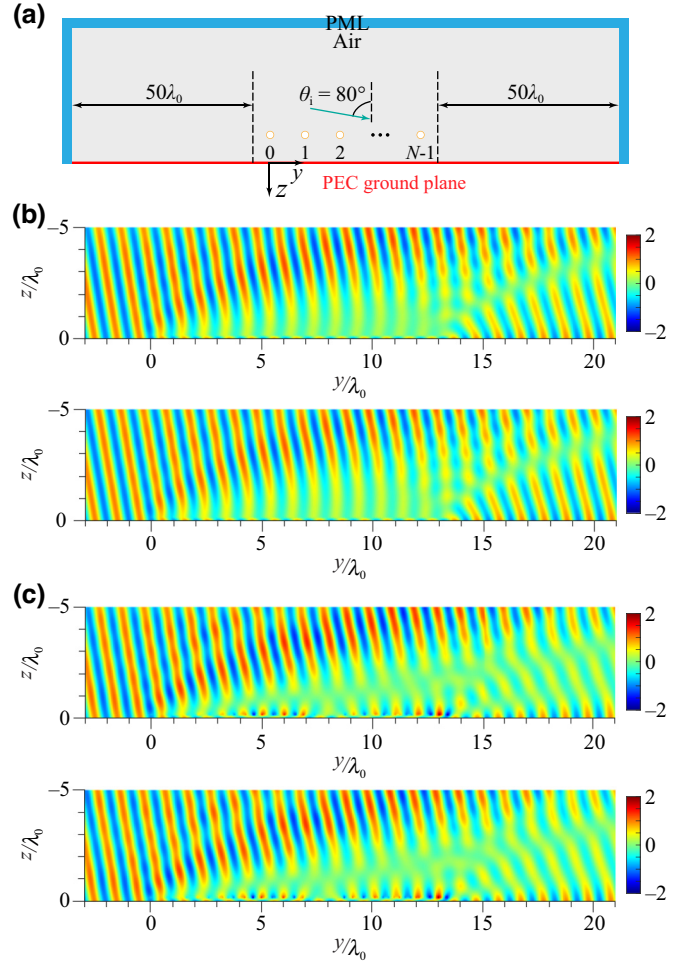


FIG. 7. (a) Schematic diagram for the COMSOL MULTIPHYSICS simulation. The simulation domain is surrounded by a perfectly matched layer (PML). The array is positioned in the center of the simulation domain. The incident angle of the plane wave is 80° . (b) Real part of the scattered electric field (with the unit of volt per meter) distribution for the reference uniform array. Numerical results (upper panel) and analytical results (lower panel). (c) Same as (b) for an array with the optimized loads. Numerical results (upper panel) and analytical results (lower panel).

The calculated absorptance as a function of the normalized frequency for different-sized absorbers is depicted in Fig. 8. As expected, we see that the optimized superdirective absorbers have a smaller frequency band, but the difference with the reference uniform absorbers is not very large. It is interesting to observe that the frequency of the maximum absorptance of the reference structures is shifted from the design frequency. This is because the effective capacitance of the whole structure decreases when the size of the top reactive layer is reduced. The decrease of effective capacitance results in an increase of the resonant frequency $\omega_{\text{res}} = 1/\sqrt{LC}$. As the absorber size increases, this frequency shift becomes smaller, as does the maximum attainable value of absorptance. Ultimately, the response

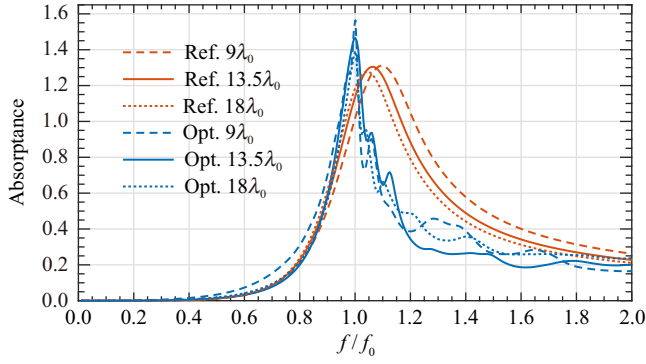


FIG. 8. Absorbance as a function of the normalized frequency for arrays of different sizes (indicated in the legend), when the incident angle is 80° . The results for the reference uniform absorbers (Ref.) are represented in red, while the curves for the optimized absorbers (Opt.) are shown in blue.

of the reference absorbers tends to the theoretical results for infinite absorbers illuminated by plane waves, with the maximum of absorbance equal to unity occurring at the design frequency f_0 , which is defined by the effective capacitance and inductance per unit length [10] instead of the parameters of whole finite-size arrays, L and C .

As stressed above, the superabsorption phenomenon is possible only in arrays with a subwavelength period. For completeness, we discuss the performance of arrays with larger periods. We consider the case when the distance between the strips and the ground plane is smaller than half the wavelength, i.e., $h < \lambda_0/2$. The overall array size is kept as $13.5\lambda_0$, and in the examples considered the distance h from the ground plane is $\lambda_0/6$. We change the geometric period d by changing the total number of strips N . Three geometric periods, i.e., $d = 0.5\lambda_0$, $d = 0.643\lambda_0$, and $d = 1.039\lambda_0$, are taken as examples, which correspond to $N = 27$, $N = 21$, and $N = 13$, respectively. The absorbance after optimization as a function of the incident angle is displayed in Fig. 9. For geometric period equal to $0.5\lambda_0$, in the corresponding infinite array only a specularly propagating mode exists for arbitrary incident angles. Perfect absorption can always be achieved, as can be seen in Fig. 9 with the solid blue and red curves, which correspond to the expected angles 0° and 75° , respectively. However, higher-order propagating modes may occur when the period is larger than $\lambda_0/2$, especially for extreme incident angles. If other propagating modes exist apart from the mode correspond to specular reflection, perfect absorption cannot be realized by the strip array, let alone superdirective absorption. For geometric period equal $0.643\lambda_0$, higher-order propagating modes occur once the incident angle is larger than 33.7° . We consider expected incident angles equal to 0° and 40° . For normal incidence, perfect absorption can be seen in Fig. 9 with the dotted blue curve. However, when the expected incident angle equals 40° , a significant

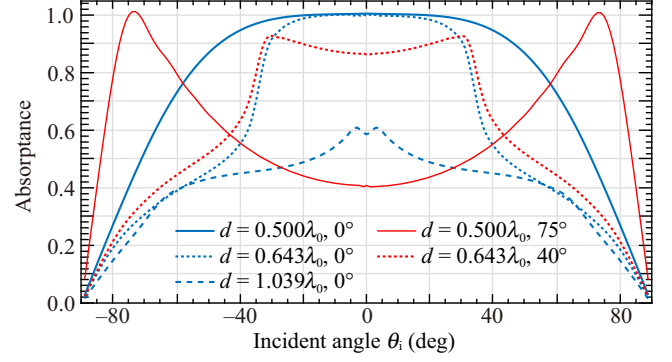


FIG. 9. Optimized results for absorbance as a function of incident angle for different periods and expected incident angles.

decrease in absorbance occurs due to the existence of higher-order propagating modes, as is seen in Fig. 9 with the dotted red curve. On further increase of the geometric period to $1.039\lambda_0$, higher-order propagating modes always exist for any incident angle, even for normal incidence, and we can never reach perfect absorption, as is seen in Fig. 9 with the dashed blue curve.

When the thickness is greater than half the wavelength, special cases may exist. The scattered propagating modes may be eliminated by the structure due to the destructive interference for some special incident angles. If the diffraction angle is θ , h should satisfy

$$2k_0h \cos \theta = 2\pi q, \quad (7)$$

where q is an integer. Hence, $h = q\pi/(k_0 \cos \theta) = q\lambda_0/(2 \cos \theta)$. This phenomenon happens only when the thickness is no less than half a wavelength. In practice, absorbers usually have subwavelength thickness. However, to illustrate this special case, we consider a simple example. The geometric period d of the strip array is approximately 1.342λ , and $h = 3\lambda_0/4$. For normal incidence, the higher-order propagating modes occur at $\theta \approx \pm 48.2^\circ$, and the corresponding $q = 1$. The absorbance as a function of incident angle is depicted in Fig. 10, where high absorbance at 0° can be observed. When the total number of strips N is ten, the array size is about $13.42\lambda_0$, which is close to the array size considered above, i.e., $13.5\lambda_0$. The absorbance at normal incidence is 87.1%, as is seen in Fig. 10 with the dashed green curve. By our increasing the number of strips, i.e., the array size, the absorbance is further increased to 93.6% and 97.6%, which correspond to $N = 20$ and $N = 50$, respectively (see the solid red curve and the dashed blue curve in Fig. 10). Ultimately, it tends to 100%, which corresponds to an infinite periodic structure. It is interesting to note there is a dip at about $\pm 48.2^\circ$, where the absorbance is zero. The external field is the superposition of the incident wave and the specular reflection from the ground plane, which gives a null at the surface of the strip array when the incident wave comes

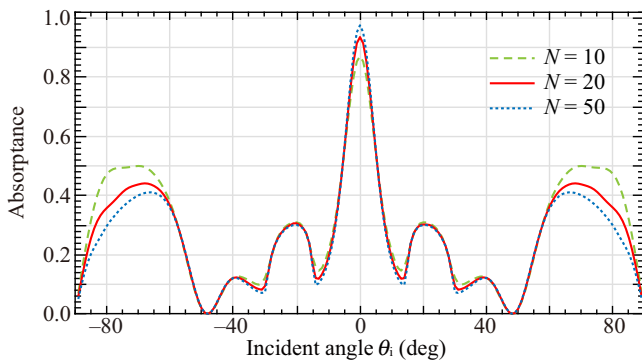


FIG. 10. Absorbance as a function of incident angle for different array sizes.

from $\pm 48.2^\circ$. Hence, the strip array cannot be excited, and it is not “visible” to the incident wave. The incident wave passes through the strip array without any reflection and then is fully specularly reflected by the ground plane.

As expected, we see that although perfect absorption (100% efficiency) can be achieved for a specific incident angle when the period is equal to $\lambda_0/2$, superabsorption is not possible in this case.

IV. CONCLUSION

We have shown that simple finite-sized geometrically periodic arrays can absorb more power than is incident on their surfaces and discussed the physical mechanism of this effect. Superabsorption is achieved by optimization of the induced surface waves, whose strong currents increase absorption in the array elements. The fields of these waves have fast variations over the array plane. Thus, the key requirement for achieving superdirective absorption is the use of arrays with a subwavelength period, to allow proper control of surface modes. Comparing the performance of conventional uniform arrays with the performance of the optimized arrays, we have found that especially for arrays designed to absorb waves at near-grazing angles, the absorbance can be significantly increased over the conventional limit of 100%. For the case of optimized arrays, both the induced currents and the load impedances change rapidly over the surface, leading to higher dissipated power. Numerical simulations of scattered fields show a shadow that is wider than the array cross section, as well as the fields of the excited surface waves which increase the dissipation process over the whole array surface. Investigation of the effects of the geometric period on absorption has revealed that the presence of higher-order propagating modes deteriorates the absorber performance. Once higher-order propagating modes occur, perfect absorption cannot be achieved with arrays of weakly directive elements (like the thin strips considered) if there is only one strip per period, except by precise tuning of the geometric period and the thickness of the substrate of the air

layer for specific incident angles. Although here we considered a simple, analytically solvable example of thin impedance-loaded strips, similar effects can be possibly achieved in arrays of arbitrary type of electrically small antennas loaded with bulk-impedance loads. Importantly, the structure can, in principle, be reconfigured for superabsorption at any angle by one changing the impedances of the loads. We hope that this study not only sheds light on the intriguing phenomenon of superunity absorbance but also presents a simple possibility for dynamically tuning absorption and enhancing the performance of absorbers in real-world applications.

ACKNOWLEDGMENTS

This work was supported in part by the China Scholarship Council under Grant No. 202106280229 and in part by the Academy of Finland under Project No. 345178.

- [1] D. Xie, X. Liu, H. Guo, X. Yang, C. Liu, and L. Zhu, A wideband absorber with a multiresonant gridded-square FSS for antenna RCS reduction, *IEEE Antennas Wirel. Propag. Lett.* **16**, 629 (2017).
- [2] J. Wen, Q. Ren, R. Peng, and Q. Zhao, Ultrabroadband saline-based metamaterial absorber with near theoretical absorption bandwidth limit, *IEEE Antennas Wirel. Propag. Lett.* **21**, 1388 (2022).
- [3] C. Fu, L. Zhang, L. Liu, S. Dong, W. Yu, and L. Han, RCS reduction on patterned graphene-based transparent flexible metasurface absorber, *IEEE Trans. Antennas Propag.* **71**, 2005 (2023).
- [4] M. R. Rakhshani, Narrowband plasmonic absorber using gold nanoparticle arrays for refractive index sensing, *IEEE Sens. J.* **22**, 4043 (2022).
- [5] H. Singh, A. Gupta, R. S. Kaler, S. Singh, and A. S. Gill, Designing and analysis of ultrathin metamaterial absorber for W band biomedical sensing application, *IEEE Sens. J.* **22**, 10524 (2022).
- [6] Y. Yashno and A. Epstein, Large-period multichannel metagratings for broad-angle absorption, in *Proc. 16th Int. Congr. Artif. Mater. Novel Wave Phenom. (Metamaterials)* (IEEE, Siena, Italy, 2022), pp. X-134–X-136.
- [7] F. Boust, T. Lepetit, and S. N. Burokur, Metagrating absorber: Design and implementation, *Opt. Lett.* **47**, 5305 (2022).
- [8] Z. Tan, J. Yi, Q. Cheng, and S. N. Burokur, Design of perfect absorber based on metagratings: Theory and experiment, *IEEE Trans. Antennas Propag.* **71**, 1832 (2023).
- [9] N. I. Landy, S. Sajuyigbe, J. J. Mock, D. R. Smith, and W. J. Padilla, Perfect metamaterial absorber, *Phys. Rev. Lett.* **100**, 207402 (2008).
- [10] Y. Ra’di, C. R. Simovski, and S. A. Tretyakov, Thin perfect absorbers for electromagnetic waves: Theory, design, and realizations, *Phys. Rev. Appl.* **3**, 037001 (2015).
- [11] X. Wang, A. Díaz-Rubio, and S. A. Tretyakov, Independent control of multiple channels in metasurface devices, *Phys. Rev. Appl.* **14**, 024089 (2020).

- [12] S. I. Maslovski, C. R. Simovski, and S. A. Tretyakov, Overcoming black body radiation limit in free space: Metamaterial superemitter, *New J. Phys.* **18**, 013034 (2016).
- [13] C. A. Valagiannopoulos, J. Vehmas, C. R. Simovski, S. A. Tretyakov, and S. I. Maslovski, Electromagnetic energy sink, *Phys. Rev. B* **92**, 245402 (2015).
- [14] G. Kirchhoff, On the relation between the radiating and absorbing powers of different bodies for light and heat, *Philos. Mag.* **20**, 1 (1860).
- [15] C. F. Bohren, How can a particle absorb more than the light incident on it?, *Am. J. Phys.* **51**, 323 (1983).
- [16] S. Tretyakov, Maximizing absorption and scattering by dipole particles, *Plasmonics* **9**, 935 (2014).
- [17] K. Ladutenko, P. Belov, O. Peña-Rodríguez, A. Mirzaei, A. E. Miroshnichenko, and I. V. Shadrivov, Superabsorption of light by nanoparticles, *Nanoscale* **7**, 18897 (2015).
- [18] S. I. Maslovski, H. R. L. Ferreira, I. O. Medvedev, and N. G. B. Brás, Superabsorbing metamaterial wormhole: Physical modeling and wave interaction effects, *Phys. Rev. B* **98**, 245143 (2018).
- [19] Z. Ruan and S. Fan, Superscattering of light from sub-wavelength nanostructures, *Phys. Rev. Lett.* **105**, 013901 (2010).
- [20] S. A. Mann and E. C. Garnett, Extreme light absorption in thin semiconductor films wrapped around metal nanowires, *Nano Lett.* **13**, 3173 (2013).
- [21] N. Mohammadi Estakhri and A. Alù, Minimum-scattering superabsorbers, *Phys. Rev. B* **89**, 121416 (2014).
- [22] Y. Li, X. Ma, X. Wang, G. Ptitsyn, M. Movahediqomi, and S. A. Tretyakov, All-angle scanning perfect anomalous reflection by using passive aperiodic gratings, *IEEE Trans. Antennas Propag.* **72**, 877 (2024).
- [23] S. Tretyakov, *Analytical Modeling in Applied Electromagnetics* (Artech House, Norwood, MA, 2003).
- [24] D. M. Pozar, *Microwave Engineering* (John Wiley & Sons, Hoboken, NJ, 2011), 4th ed.
- [25] V. A. Rozov and S. A. Tretyakov, Diffraction of plane electromagnetic waves by a semi-infinite grid of parallel conductors, *Radioeng. Electron. Phys.* **26**, 6 (1981).